Spectrotemporal shaping of itinerant photons via distributed nanomechanics

Linran Fan, Chang-Ling Zou, Na Zhu and Hong X. Tang

Efficient phase manipulation of light is the cornerstone of many advanced photonic applications¹⁻⁴. However, the pursuit of compact, broadband and deep phase control of light has been hindered by the finite nonlinearity of the optical materials available for integrated photonics^{5,6}. Here, we propose a dynamically driven photonic structure for deep phase manipulation and coherent spectrotemporal control of light based on distributed nanomechanics. We experimentally demonstrate the quasi-phase-matched interaction between stationary mechanical vibration and itinerant optical fields, which is used to generate an on-chip modulated frequency comb over 1.15 THz (160 lines), corresponding to a phase modulation depth of over 21.6 π . In addition, an optical time-lens effect induced by mechanical vibration is realized, leading to optical pulse compression of over 70-fold to obtain a minimum pulse duration of 1.02 ps. The high efficiency and versatility make such mechanically driven dynamic photonic structures ideal for realizing complex optical control schemes, such as lossless non-reciprocity, frequency division optical communication1 and optical frequency comb division8.

The pursuit of more efficient active control of the optical phase has never ceased. Besides its paramount influence in traditional optical communications^{1,2}, it also lays down the foundation for modern optical spectrotemporal manipulation for both classical and quantum applications^{3,4}. Advanced functions such as ultrafast temporal imaging^{9,10}, the effective magnetic field of light^{7,11,12} and optical non-reciprocity¹³⁻¹⁵ have been proposed and demonstrated. To further improve performance, on-chip integration of advanced spectrotemporal control methods with nanoscale structures is highly desired. This will not only provide a compact footprint and scalability, but will also enable critical benefits including precise dispersion control and significant field enhancement due to the orders of magnitude reduction in mode volume, as demonstrated by the rapid recent development of optical microcombs based on the Kerr effect^{16,17}. However, the required optical nonlinearity for spectrotemporal control is difficult to implement at the nanoscale because of issues with material availability, and the achievable nonlinearity is limited to the material's intrinsic nonlinearity^{5,6,18}. While promising results have been achieved with approaches based on three-wave and four-wave mixing¹⁹⁻²¹, spectrotemporal control with microwave signals is highly advantageous due to its direct interface with microwave circuits, elimination of the need for strong optical pumps and the high flexibility in achieving complex control schemes.

A strong interaction between mechanical vibration and optical fields has been proven in the context of optomechanics as an efficient alternative method for optical phase control²². The tight mode confinement and mechanical resonance enhancement, in particular, can lead to a phase control efficiency surpassing the intrinsic material electrooptic property²³. Effects such as photon frequency

shift²³, optical delay^{24,25} and Brillouin amplification²⁶ have been realized. However, optical cavities or limited interaction lengths are used to mitigate the large velocity mismatch between the mechanical vibration and optical fields^{23–26}. Therefore, deep and broadband control of optical spectrotemporal properties with mechanics has not been demonstrated so far and remains a significant challenge in the development of efficient on-chip photon control systems.

In this Letter we demonstrate efficient on-chip spectrotemporal shaping of itinerant photons enabled by nanomechanics driven at microwave frequencies. The co-localization of mechanical vibration and optical fields in piezoelectric waveguides provides a strong phonon–photon interaction, which is used for efficient and low-loss optical phase modulation. The quasi-phase matching between mechanical vibration and optical propagation is realized by fabricating alternating suspended and clamped waveguides on a single chip. By actuating the mechanical vibration with the piezoelectric effect, a phase modulation depth around 21.6π has been achieved over an optical bandwidth of 20 nm. Based on the efficient phase control, a modulated optical comb over $1.15\,\text{THz}$ (160 lines) and a time lens with 70-fold compression ratio have been demonstrated.

The interaction between mechanical vibration and the optical fields in a waveguide can be interpreted as a second-order nonlinear process, so the phase-matching condition among the driving optical field, mechanical vibration and modulated optical field should be satisfied²⁷. Here, the standing mechanical vibration with zero momentum is utilized, so the momentum of the driving and modulated optical fields should match each other. Therefore, additional momentum should be introduced to compensate for the momentum mismatch due to optical linear dispersion in the waveguide. In this way, the interactions from each section can accumulate constructively to produce enhanced interaction in a travelling wave configuration (Fig. 1a). The additional momentum can be realized by fabricating alternating suspended and clamped waveguides (Fig. 1b); only the suspended waveguides can be driven efficiently and contribute to the total interaction. To compensate for the momentum difference $\delta k = n_o \omega_m / c$, the length of both suspended and clamped waveguide sections should be

$$L = \frac{\pi}{\delta k} = \frac{c}{n_{\rm g}} \frac{\pi}{\omega_{\rm m}} \tag{1}$$

with $n_{\rm g}$ is the optical group index, $\omega_{\rm m}$ is the mechanical angular frequency and c is the speed of light in vacuum (Supplementary Section 1). To achieve robust hybrid waveguides with small footprint and low insertion loss, we designed spiral arrays with a ridge waveguide to confine both the optical and mechanical modes (Fig. 1b). In the suspended waveguide, the thickness of the mechanical mode deforms the waveguide boundary and changes the effective refractive index of the transverse magnetic (TM) optical mode,

LETTERS NATURE PHOTONICS

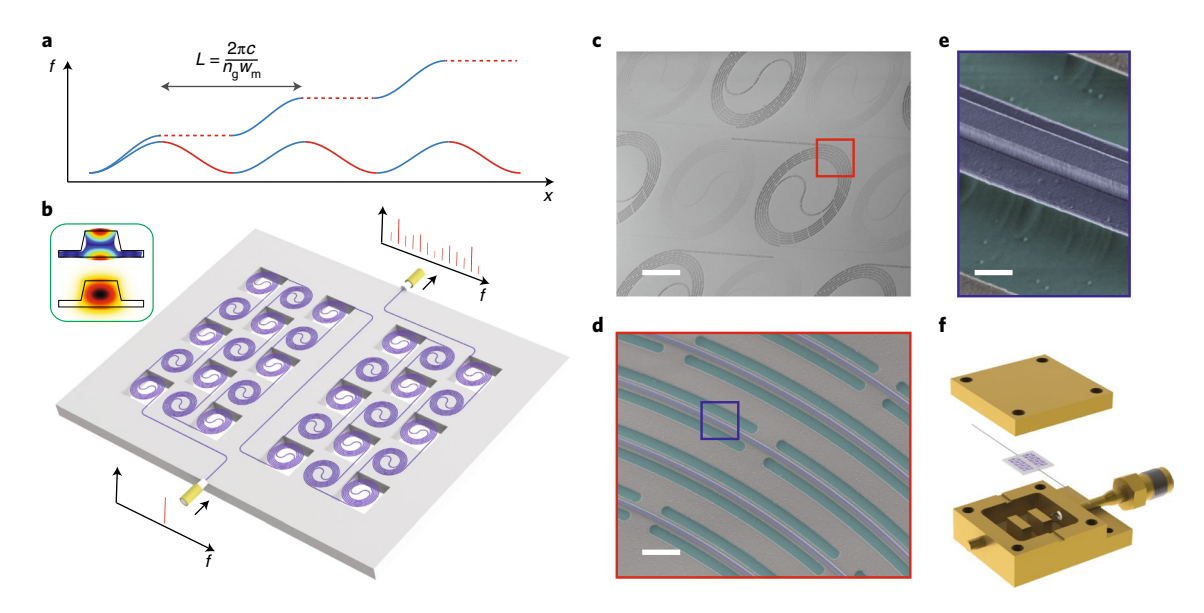


Fig. 1 | Integrated deep phase modulation based on a distributed nanomechanical-photonic waveguide. a, Principle of quasi-phase matching. While the mechanical resonator oscillates periodically, propagating optical fields experience a half positive (blue solid line) and half negative (red solid line) phase change. The net effect over a long interaction length cancels. By turning off the negative part (red dashed line), optical fields experience only the positive phase change, which accumulates constructively and leads to an enhanced net interaction. **b**, Schematic of the quasi-phase-matching device. The waveguide spirals are suspended and clamped alternately, and each waveguide spiral has a length of 9.1mm. The deformed mechanical mode (top) and TM optical mode (bottom) are shown in the inset. **c**, Scanning electron microscopy (SEM) image of the fabricated device. Scale bar, 200 μm. **d**, SEM image of the suspended spiral waveguide (red square in **c**). Scale bar, 15 μm. **e**, SEM image of the suspended ridge waveguide (blue square in **d**). Scale bar, 1.5 μm. **f**, Schematic of the device packaging.

leading to a strong interaction between the optical fields and the mechanical vibration. The use of a ridge waveguide also eliminates the optical scattering loss at the interface between the suspended and clamped waveguides.

Based on the design, the waveguides were fabricated from an aluminium nitride (AlN) layer on a silicon dioxide (SiO2) layer on a sapphire wafer, with alternating suspended and clamped spiral waveguide arrays to achieve the quasi-phase matching (Fig. 1c; for further explanation see Methods). A sapphire substrate was chosen instead of silicon to eliminate microwave losses induced by room-temperature free carriers. The suspended waveguides are supported by a pair of tethers every 100 µm to provide robust support and also to minimize mechanical clamping losses (Fig. 1d,e). Each waveguide spiral has a length of 9.1 mm (obtained from equation (1)), with a footprint of $0.6 \times 0.6 \,\mathrm{mm}^2$. When placed in a threedimensional (3D) copper cavity, the mechanical mode is actuated by a microwave electric field via the piezoelectric effect of the AlN (Fig. 1f). Light is coupled into and out of the device using facet coupling with two lens fibres, and the microwave signal is delivered through a magnetic probe loop connected to a coaxial subminiature version A (SMA) cable.

The mechanical mode is characterized by piezoelectrically exciting and optically detecting the mechanical motion by using a weak Fabry–Pérot interferometer formed between the waveguide facets²8. The measured spectrum is shown in Fig. 2a, with the resonant frequency of $\omega_{\rm m}=2\pi\times7.15\,{\rm GHz}$ and linewidth of $\kappa_{\rm m}=2\pi\times3.41\,{\rm MHz}$. The microwave cavity is characterized by measuring the microwave reflection spectrum through a magnetic probe loop. Two copper pedestals are used to maximize the overlap between microwave field and mechanical vibration (Fig. 2c). A copper rod is inserted into the cavity to tune the microwave resonant frequency to match the mechanical frequency. The critically coupled anti-symmetric mode at $\omega_{\rm mw}=2\pi\times7.15\,{\rm GHz}$ is realized by adjusting the copper rod position, and the total linewidth is $\kappa_{\rm mw}=2\pi\times7.17\,{\rm MHz}$, as shown in Fig. 2b (Supplementary Section 2).

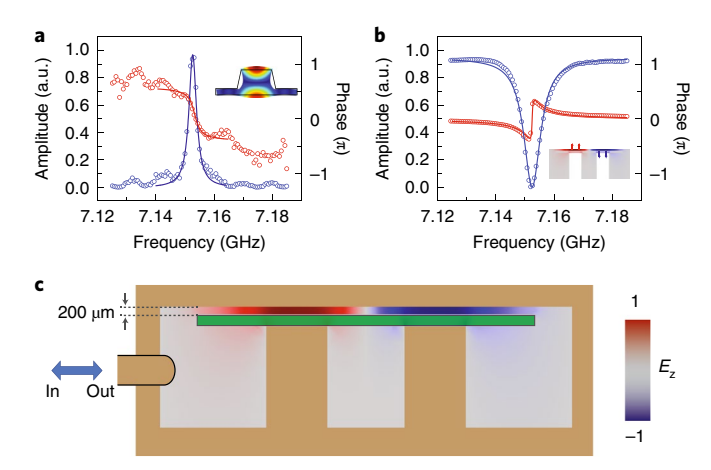


Fig. 2 | Device characterization. a, Mechanical resonance. The measured amplitude (blue circles) and phase (red circles) are fitted by a Lorentzian shape (solid line), corresponding to a centre frequency of 7.15 GHz and linewidth of 3.41 MHz. Inset: simulated profile of the mechanical mode. **b**, Reflection spectrum of the antisymmetric microwave resonance. The measured amplitude (blue circles) and phase (red circles) are fitted by a Lorentzian shape (solid line), leading to a centre frequency of 7.15 GHz and linewidth of 7.17 MHz. Inset: simulated electric field distribution. **c**, Cross-section of the device. Two pedestals in the 3D cavity (brown) confine the electric field, and the simulated *z*-direction electric field of the antisymmetric mode is shown as the colour plot. The π phase change of the electric field between the two pedestals is compensated by the on-chip optical delay. The sapphire chip (green) is placed on the pedestals so that the mechanical vibration is driven most efficiently. A copper rod is used to precisely tune the microwave frequency.

We first demonstrate the ultrawide modulated comb generation by utilizing the deep phase modulation resulting from the quasi-phase-matched interaction between the optical fields and

NATURE PHOTONICS LETTERS

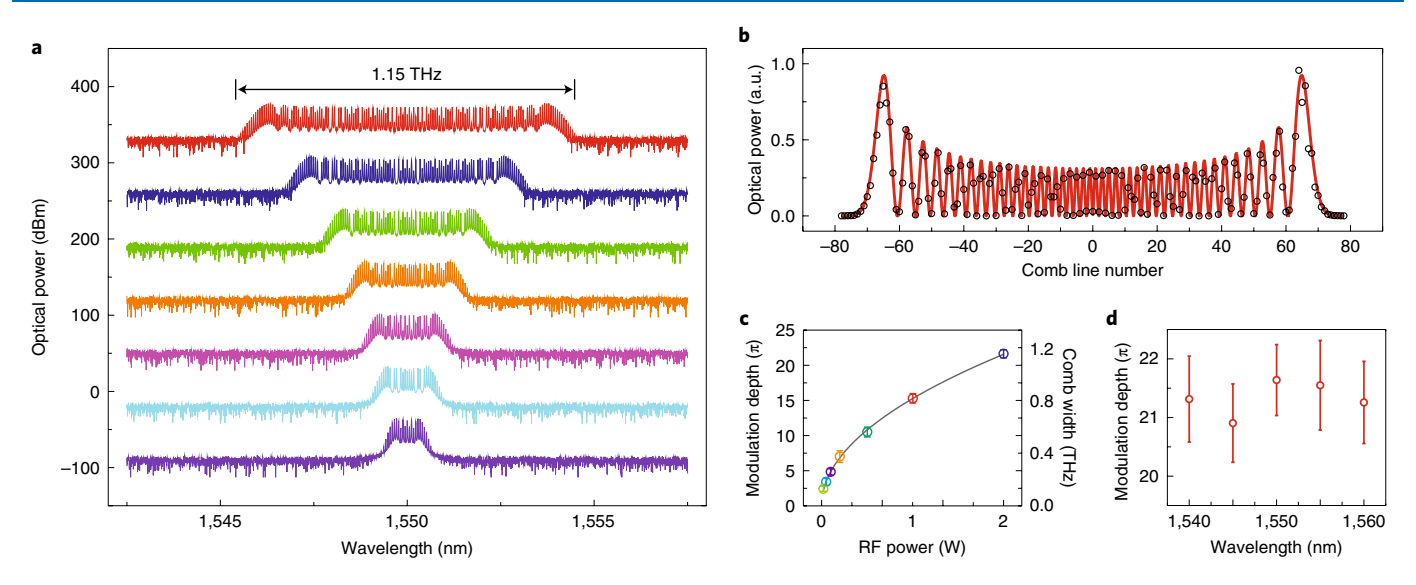


Fig. 3 | On-chip modulated comb generation. a, Measured output optical spectra for input microwave powers of 2 W (red), 1 W (blue), 0.5 W (green), 0.2 W (orange), 0.1 W (pink), 0.05 W (cyan) and 0.02 W (purple). The spectra are offset for clarity. b, Modulated comb power profiles with 2 W microwave power. The measured power of each individual comb line (black circle) is fitted with the square of the Bessel function of the first kind (red line), with modulation depth and total power as independent parameters. The modulation depth is estimated as $(21.6 \pm 0.3)\pi$. c, Modulation depth and comb width dependence on input microwave power. The solid line is the fitted result with $\Delta \phi = \eta \sqrt{P}$. d, Modulation depth with different input optical wavelengths. The input microwave power is fixed at 2 W. The 95% confidence interval error bars are dervived from the Bessel function (b) fitting of the spectrum.

the mechanical vibration. Continuous-wave (c.w.) light and microwaves are launched into the device through the lens fibre and SMA connector, respectively. A strong electric field is formed across the device, leading to large-amplitude mechanical vibration, which is further boosted, simultaneously, by the mechanical resonance and microwave resonance. The mechanical vibration modulates the optical phase in each suspended waveguide spiral, which accumulates constructively to generate deep phase modulation. By fixing the input microwave frequency ω_d at $2\pi \times 7.15\,\mathrm{GHz}$ and gradually increasing the input microwave power, the modulated comb bandwidth increases accordingly (Fig. 3a). With a maximum input microwave power of 2W, the modulated comb can be expanded over a bandwidth of 1.15 THz (160 lines). The spectrum profile of the modulated comb follows the square of the Bessel function of the first kind (Supplementary Section 1). Distinct from the Kerr optical combs generated in microcavities²⁹, no chaos process will emerge in the generation of modulated optical combs, and comb noise at radiofrequencies (RF) is determined by the technical noise of the laser and the RF drive³⁰ (Supplementary Section 3). By fitting the power of individual comb lines to Bessel functions, a phase modulation depth as large as $\Delta \phi = (21.6 \pm 0.3)\pi$ can be estimated with the uncertainty from the fitting error (Fig. 3b). Because the phase modulation depth is proportional to the amplitude of the mechanical amplitude, which in turn is proportional to the square root of the RF drive power P, we obtain the modulation efficiency $\eta = \frac{\Delta \phi}{\sqrt{D}} \approx 15.3\pi / \sqrt{W}$ (Fig. 3c). As no optical cavity is involved in the process, this device can operate in a broad optical bandwidth, as shown in Fig. 3d. The input wavelength is varied from 1,540 nm to 1,560 nm, and no obvious modulation depth change is observed. In principle, any wavelength within the AlN transparent window from the visible to the mid-infrared can be utilized to produce a modulated comb31.

The deep optical phase modulation driven by nanomechanics can also be used for temporal domain manipulation of optical fields. Here, we realize the optical pulse compression based on the timelens principle (Supplementary Section 4)^{9,32}. With c.w. light input, we first deliver periodically modulated optical pulses (duration of $\tau_0 = \pi/\omega_d \approx 70 \, \mathrm{ps}$) into the device with a Mach–Zehnder electrooptic

modulator (Fig. 4a). The mechanical mode is driven by the microwave signal from the same source, albeit with π phase difference from the Mach-Zehnder modulator. In this way, the optical pulses gain a chirped phase in the time domain, imprinted by the device. Then, a 300 m single-mode fibre is used to compensate the dispersion, compressing the optical pulses in the time domain. As shown in Fig. 4b, a flat-top comb is generated with a driving microwave power of 2 W. In contrast to the varying comb profile with pure phase modulation (Fig. 3b), the variation in comb line power is smaller than 1 dB over a bandwidth of 350 GHz (Fig. 4c). The temporal profiles of the compressed optical pulses are characterized by second-harmonic generation frequency-resolved optical gating (SHG-FROG)33, which shows an anticorrelation intensity full-width at half-maximum (FWHM) of 1.37 ± 0.03 ps, corresponding to pulse duration $\tau_1 = 1.02 \pm 0.02$ ps (Fig. 4d)³². The uncertainty in the pulse duration is obtained by multiple measurements. Compared with the initial pulse duration $\tau_0 \approx 70$ ps, the optical pulses are compressed in the time domain by about 70-fold.

While further improvement of the phase modulation efficiency can be achieved by cascading more waveguide spirals on the same chip, the mechanical frequency spatial inhomogeneity (that is, the mechanical frequencies varying in different areas due to variation in the wafer thickness, film stress and fabrication process) should also be addressed. By engineering the waveguide geometry accordingly based on prior knowledge of the wafer inhomogeneity, we expect that the standard deviation of the mechanical frequencies can be controlled to be smaller than the linewidth (Supplementary Section 5).

Compared with a conventional modulation method using bulk nonlinear crystals such as LiNbO₃, our approach based on mechanical vibration in AlN waveguides allows high optical power handling in both the visible and infrared regime (Supplementary Section 6), without the limit imposed by the photorefractive effect³⁴. The $V_\pi \cdot L$ of our device is $(17.3 \pm 0.3) \, V$ cm, which is more than one order of magnitude improvement compared with pure electrooptic modulation in AlN³¹. We expect that our method can also be applied to LiNbO₃ nanophotonic structures, leading to $V_\pi \cdot L$ values far below 1 V cm. Moreover, this device can be easily integrated with other

LETTERS NATURE PHOTONICS

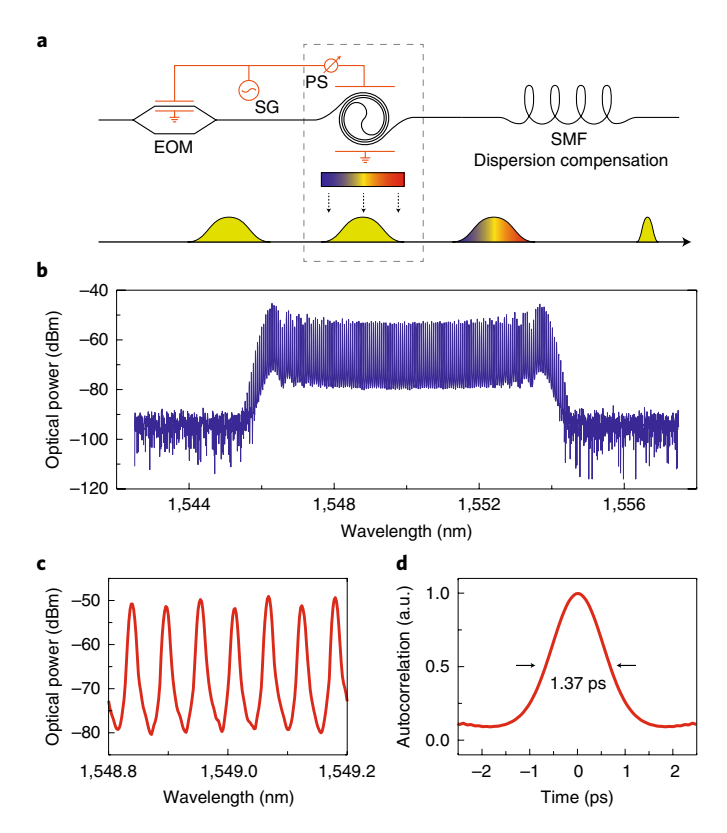


Fig. 4 | Pulse compression with a mechanical time lens. a, Measurement set-up. Wide optical pulses are first generated by a Mach-Zehnder electro-optic modulator (EOM), then sent into the device for phase chirping and then into a single-mode fibre (SMF) for dispersion compensation. Microwave signals for the EOM and device are provided by the same signal generator (SG), and the phase difference is controlled by a phase shifter (PS). **b**, Measured output optical spectrum of the flat-top comb. **c**, Enlarged view of the output optical spectrum. The power variation among comb lines is below 1dB, and the linewidth is limited by the resolution of the optical spectrum analyser. **d**, Autocorrelation intensity of output optical pulses measured with SHG-FROG. The FWHM is 1.37 ps, corresponding to a pulse width of 1.02 ps, fitted with a sinc pulse shape.

on-chip optical components to produce novel optical control paradigms. For example, a Kerr optical comb has been generated with the same material platform with a free spectral range (FSR) on the order of 100 GHz and even beyond 1 THz (ref. ³⁵). Deep mechanical modulation can be utilized to aid FSR locking with low-speed photodetectors. By locking the modulated comb driven by nanomechanics with the Kerr optical comb, a wide optical comb with small FSR interpolation can be realized, which is critical in comb spectroscopy and precision metrology.

In addition, our device consists of arrays of active and passive sections to control both phase and modulation depth. Different configurations of phase and modulation depth in different sections can also be realized. This is critically important for further increasing the capability of photonic integrated circuits with temporal modulation techniques. Many methods to break the performance limits of conventional photonics have been theoretically proposed, including an effective magnetic field for photons, optical non-reciprocity without bulky magnetics, lossless on-chip isolators, time reversal of optical pulses and arbitrary control of optical flows^{7,11,12,36}. The deep phase modulation and flexible device configuration described here promise a platform to demonstrate these theoretical proposals.

In conclusion, we have demonstrated efficient on-chip optical phase control using a quasi-phase-matched interaction between an itinerant optical field and mechanical vibration. The quasiphase matching is realized with alternating suspended and clamped nanoscale waveguides on a single chip, allowing strong interaction over a large optical bandwidth. The optical modulated comb and time lens are utilized as examples to demonstrate the efficiency and versatility of our device, and we anticipate more advanced photon control paradigms to be realized with higher efficiency and smaller footprint. This work should provide an efficient method for on-chip optical spectrotemporal control, paving the way to realize a complex photon processing platform.

Online content

Any methods, additional references, Nature Research reporting summaries, source data, statements of data availability and associated accession codes are available at https://doi.org/10.1038/s41566-019-0375-9.

Received: 18 June 2018; Accepted: 30 January 2019; Published online: 11 March 2019

References

- 1. Ho, K.-P. *Phase-Modulated Optical Communication Systems* (Springer Science & Business Media, Berlin, 2005).
- Agrawal, G. P. Fiber-optic Communication Systems Vol. 222 (John Wiley & Sons, New York, NY, 2012).
- Lu, L., Joannopoulos, J. D. & Soljačić, M. Topological photonics. Nat. Photon. 8, 821–829 (2014).
- Sounas, D. L. & Alù, A. Non-reciprocal photonics based on time modulation. Nat. Photon. 11, 774–783 (2017).
- Leuthold, J., Koos, C. & Freude, W. Nonlinear silicon photonics. Nat. Photon. 4, 535–544 (2010).
- Reed, G. T., Mashanovich, G., Gardes, F. & Thomson, D. Silicon optical modulators. *Nat. Photon.* 4, 518–526 (2010).
- Fang, K., Yu, Z. & Fan, S. Realizing effective magnetic field for photons by controlling the phase of dynamic modulation. *Nat. Photon.* 6, 782–787 (2012)
- Li, J., Yi, X., Lee, H., Diddams, S. A. & Vahala, K. J. Electro-optical frequency division and stable microwave synthesis. *Science* 345, 309–313 (2014).
- 9. Kolner, B. H. & Nazarathy, M. Temporal imaging with a time lens. *Opt. Lett.* 14, 630–632 (1989).
- Karpiński, M., Jachura, M., Wright, L. J. & Smith, B. J. Bandwidth manipulation of quantum light by an electro-optic time lens. *Nat. Photon.* 11, 53–57 (2017).
- Fang, K., Yu, Z. & Fan, S. Photonic Aharonov–Bohm effect based on dynamic modulation. *Phys. Rev. Lett.* 108, 153901 (2012).
- Tzuang, L. D., Fang, K., Nussenzveig, P., Fan, S. & Lipson, M. Non-reciprocal phase shift induced by an effective magnetic flux for light. *Nat. Photon.* 8, 701–705 (2014).
- Yu, Z. & Fan, S. Complete optical isolation created by indirect interband photonic transitions. *Nat. Photon.* 3, 91–94 (2009).
- Feng, L. et al. Nonreciprocal light propagation in a silicon photonic circuit. Science 333, 729–733 (2011).
- Sounas, D. L., Caloz, C. & Alu, A. Giant non-reciprocity at the subwavelength scale using angular momentum-biased metamaterials. *Nat. Commun.* 4, 2407 (2013).
- 16. Vahala, K. J. Optical microcavities. Nature 424, 839-846 (2003).
- Kippenberg, T. J., Holzwarth, R. & Diddams, S. Microresonator-based optical frequency combs. Science 332, 555–559 (2011).
- Wooten, E. L. et al. A review of lithium niobate modulators for fiber-optic communications systems. *IEEE J. Sel. Topics Quantum Electron.* 6, 69–82 (2000).
- Bennett, C. V., Scott, R. P. & Kolner, B. H. Temporal magnification and reversal of 100 Gb/s optical data with an up-conversion time microscope. *Appl. Phys. Lett.* 65, 2513–2515 (1994).
- Bennett, C. V. & Kolner, B. H. Principles of parametric temporal imaging. Part I. System configuration. *IEEE J. Quant. Electron* 36, 430–437 (2000).
- Salem, R. et al. Optical time lens based on four-wave mixing on a silicon chip. Opt. Lett. 33, 1047–1049 (2008).
- Aspelmeyer, M., Kippenberg, T. J. & Marquardt, F. Cavity optomechanics. Rev. Mod. Phys. 86, 1391 (2014).
- Fan, L. et al. Integrated optomechanical single-photon frequency shifter. Nat. Photon. 10, 766–770 (2016).
- Weis, S. et al. Optomechanically induced transparency. Science 330, 1520–1523 (2010).

NATURE PHOTONICS LETTERS

- Safavi-Naeini, A. H. et al. Electromagnetically induced transparency and slow light with optomechanics. *Nature* 472, 69–73 (2011).
- 26. Kittlaus, E. A., Shin, H. & Rakich, P. T. Large Brillouin amplification in silicon. *Nat. Photon.* **10**, 463–467 (2016).
- 27. Boyd, R. W. Nonlinear Optics (Academic Press, Cambridge, MA, 2003).
- Li, M. et al. Harnessing optical forces in integrated photonic circuits. Nature 456, 480–484 (2008).
- 29. Herr, T. et al. Temporal solitons in optical microresonators. *Nat. Photon.* **8**, 145–152 (2014).
- Ishizawa, A. et al. Phase-noise characteristics of a 25-GHz-spaced optical frequency comb based on a phase- and intensity-modulated laser. Opt. Express 21, 29186–29194 (2013).
- Xiong, C. et al. Aluminum nitride as a new material for chip-scale optomechanics and nonlinear optics. New J. Phys. 14, 095014 (2012).
- 32. Wu, R., Supradeepa, V., Long, C. M., Leaird, D. E. & Weiner, A. M. Generation of very flat optical frequency combs from continuous-wave lasers using cascaded intensity and phase modulators driven by tailored radio frequency waveforms. *Opt. Lett.* 35, 3234–3236 (2010).
- 33. DeLong, K., Trebino, R., Hunter, J. & White, W. Frequency-resolved optical gating with the use of second-harmonic generation. *J. Opt. Soc. Am. B* 11, 2206–2215 (1994).
- Bryan, D., Gerson, R. & Tomaschke, H. Increased optical damage resistance in lithium niobate. Appl. Phys. Lett. 44, 847–849 (1984).
- Jung, H., Stoll, R., Guo, X., Fischer, D. & Tang, H. X. Green, red, and IR frequency comb line generation from single IR pump in AlN microring resonator. Optica 1, 396–399 (2014).
- Fang, K. & Fan, S. Controlling the flow of light using the inhomogeneous effective gauge field that emerges from dynamic modulation. *Phys. Rev. Lett.* 111, 203901 (2013).

Acknowledgements

We acknowledge funding support from an LPS/ARO grant (W911NF-14-1-0563), an AFOSR MURI grant (FA9550-15-1-0029), a NSF EFRI grant (EFMA-1640959) and the DARPA SCOUT programme, as well as the Packard Foundation. The facilities used were supported by Yale Institute for Nanoscience and Quantum Engineering and NSF MRSEC DMR 1119826. We thank L. Jiang for discussions, and M. Power, M. Rooks and L. Frunzio for assistance with device fabrication.

Author contributions

H.X.T., L.F. and C.-L.Z. conceived the experiment. L.F. fabricated the device. N.Z. fabricated the 3D cavity. L.F. and N.Z. performed the experiment. L.F. and C.-L.Z. analysed the data. All authors contributed to writing the manuscript. H.X.T. supervised the work.

Competing interests

The authors declare no competing interests.

Additional information

Supplementary information is available for this paper at https://doi.org/10.1038/ \pm 41566-019-0375-9.

Reprints and permissions information is available at www.nature.com/reprints.

Correspondence and requests for materials should be addressed to H.X.T.

Publisher's note: Springer Nature remains neutral with regard to jurisdictional claims in published maps and institutional affiliations.

© The Author(s), under exclusive licence to Springer Nature Limited 2019

LETTERS NATURE PHOTONICS

Methods

Device fabrication. The device was fabricated from 800-nm-thick AlN on a $2\text{-}\mu\text{m}$ -thick SiO_2 layer on a sapphire wafer. First, $300\,\text{nm}$ SiO_2 was deposited using plasma-enhanced chemical vapour deposition. Nanophotonic structures, including microrings and waveguides, were then patterned with electron-beam lithography (EBL) using ma-N 2403 resist, subsequently transferred to the SiO_2 layer by fluorine-based reactive ion etching (RIE), then transferred to the AlN layer by chlorine-based RIE. In this step, only 600 nm of the 800 nm AlN was initially etched. In a second EBL step using ZEP520A resist, the release window was defined, followed by RIE of the remaining 200 nm AlN. Finally, the waveguides were released in buffered oxide etchant.

Optical loss measurement. The optical losses of our device consist of two parts: (1) coupling loss between the waveguides and fibres and (2) waveguide

propagation loss. The coupling loss was measured with multiple calibration devices with short length and no released structure. The propagation loss of the calibration devices was neglected, and the total coupling loss, including both input and output, was estimated as $8\pm0.9\,\mathrm{dB}$. The waveguide propagation loss was estimated by measuring the quality factor of test devices (racetrack optical resonators with half released and half unreleased waveguides). The intrinsic quality factor Q_i was estimated as $(440\pm40)\times10^3$, giving a propagation loss of

$$\alpha = \frac{10 \log_{10} e \times 2\pi n_g}{Q_i \lambda} = 0.91 \pm 0.08 \text{ dB cm}^{-1}$$

Data availability

The data that support the plots within this paper and other findings of this study are available from the corresponding author upon reasonable request.